WILEY-VCH

LETTER

Cell perforation mediated by plasmonic bubbles generated by a single near infrared femtosecond laser pulse

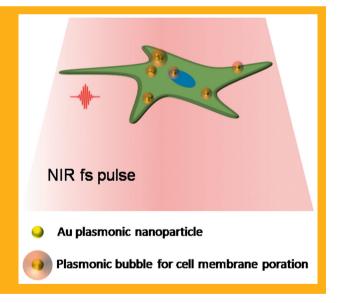*Christos Boutopoulos*[1, 2]*, Eric Bergeron*[1]*, and Michel Meunier**[*, 1]

[1] Laser Processing and Plasmonics Laboratory, Engineering Physics Department, École Polytechnique de Montréal, Montréal, Québec, H3C 3A7, Canada
[2] SUPA, School of Physics and Astronomy, University of St. Andrews, North Haugh, St. Andrews, KY16 9SS, UK

We report on transient membrane perforation of living cancer cells using plasmonic gold nanoparticles (AuNPs) enhanced single near infrared (NIR) femtosecond (fs) laser pulse. Under optimized laser energy fluence, single pulse treatment ($\tau = 45$ fs, $\lambda = 800$ nm) resulted in 77% cell perforation efficiency and 90% cell viability. Using dark field and ultrafast imaging, we demonstrated that the generation of submicron bubbles around the AuNPs is the necessary condition for the cell membrane perforation. AuNP clustering increased drastically the bubble generation efficiency, thus enabling an effective laser treatment using low energy dose in the NIR optical therapeutical window.

Schematic representation of single femtosecond laser pulse plasmonic bubble generation in the vicinity of a cell.

1. Introduction

The effective delivery of exogenous genetic material in living mammalian cells (cell transfection) offers a great potential for developing revolutionary gene therapy, which aims to identify and treat diseases that result from mutated genes [1]. Up to date, the use of viral vectors is the most efficient *in vivo* cell transfection method allowing relatively stable long-term gene expression. However, the use of viral vectors raises concerns about immunogenecity, infection transmission and mutagenicity risks. Thus, a variety of alternative methods has been developed for delivering biomolecules by physical disruption of the cell

* Corresponding author: e-mail: michel.meunier@polymtl.ca

membrane. These include either single cell techniques, such as injection [2] and optoinjection [3] or high throughput techniques such as electroporation [4].

During the last decade, there is an increased interest towards the use of laser irradiated gold nanoparticles (AuNPs) for the perforation of the cell membrane [5–14]. In this approach, AuNPs are deposited on the cells and irradiated with a slightly focused pulsed laser beam to induce localized transient disruption of the phospholipid membrane. When on-resonance laser irradiation is used, the AuNPs act as "nanoheaters". The resulting perforation mechanism has been mainly linked to the generation of plasmonic bubbles (PBs) on the cell membrane [9]. Recently, off-resonance laser irradiation of AuNPs has been employed for cell membrane perforation and transfection using either femtosecond (fs) [7, 12, 13] or nanosecond (ns) laser pulses [10]. Cell perforation with ns off-resonance pulses requires a high laser dose and it has been mainly linked to thermal effects [10]. Interestingly, off-resonance fs irradiation of AuNPs can lead to a chain of physical events in the nanoscale, involving near-field enhancement, nanoplasma generation and PB generation [15]. PB generation has been speculated to be dominant for the membrane perforation considering either numerical simulations or the optical breakdown threshold for ultrafast 800 nm pulses in water [7]. However, current literature lacks of studies dealing with *in situ* monitoring of PB generation during off-resonance fs irradiation of living cells. Moreover, multiple laser pulse irradiation has been employed so far, which limits threshold investigations and possibly introduces additional accumulative effects. Thus, the membrane perforation mechanism remains an open topic that has to be addressed in order to achieve further optimization of the technique.

In this work, we employed plasmonic AuNPs enhanced single near infrared (NIR) fs pulse to cause local and transient perforation of cell membranes. We used *in situ* dark field (DF) imaging and scanning electron microscopy (SEM) to investigate the presence of AuNPs in cell samples and ultrafast imaging to detect PB generation with nanoscale temporal and spatial resolution. We focused in the sub-threshold laser fluence regime for cell perforation, where the PB generation was correlated with the membrane perforation.

2. Experimental

MDA-MB-231 human breast cancer cells were seeded onto glass bottom dishes (1×10^5 cells, 19.63 cm², MatTek) and grown in Dulbecco's Modified Eagle's Medium (DMEM) supplemented with antibiotics (100 units/mL penicillin and 100 µg/mL streptomycin, Invitrogen) and 10% fetal bovine serum (FBS, Invitrogen) in a humidified incubator at 37 °C under a 5% CO_2 atmosphere. When cells reached 80% confluence, they were washed once with phosphate-buffered saline (PBS, Sigma-Aldrich). The cells were then incubated with 8 µg/mL 100 nm AuNPs (Nanopartz, A11-100-PBS, polydispersity index: 6%, pH = 7, zeta potential: –38 mV, surface plasmon resonance peak: 584 nm) in 2 mL culture medium during 2 h. Considering the dish area (19.63 cm²), we calculated an injection of 0.81 AuNPs/µm². We measured the average cell area to be 458 µm² and we extracted the initial number of AuNPs per cell to be 371. Cells were washed three times with PBS prior to the laser treatment.

A Ti : Sapphire laser (6 mJ/pulse, 45 fs, 800 nm, 1 kHz, Spectra-Physics) was used for the cell perforation. The beam was focused from the back side of the glass bottom dish using a long focal length lens ($f = 750$ mm). A Gaussian beam profile was measured with a spot diameter of 0.625 mm (defined at $1/e^2$). Average fluence is considered in our analysis. Laser treatment was carried out using xy motorized translation stage to irradiate multiple 2 mm × 0.5 mm areas per dish. The laser repetition rate was 3 Hz and the translation stage velocity was 1.5 mm/s to achieve single pulse treatment with 20% pulse to pulse spatial overlap.

Prior to laser treatment, the cell membranes were stained with a green dye (Alexa Fluor 488 conjugate of wheat germ agglutinin (WGA), Invitrogen) in order to facilitate the cell counting.

The cell perforation rate was estimated by measuring the uptake of a red fluorescent dye (1.5 µM propidium iodide, PI, Sigma-Aldrich). We added PI in the cell culture medium (phenol red-free DMEM containing 10% FBS) 5 min before laser treatment. 5 min after the laser treatment, the cells were washed twice with PBS. Afterwards, the cells were kept 0.5 h in the incubator prior to fluorescence microscopy observation. The cell perforation rate at a given laser fluence was calculated as the ratio of red cells over green cells multiplied by the corresponding viability rate:

Perforation rate (%) = (No. of red cells/No. of green cells) x viability rate (%), time of PI addition: 5 min before laser treatment.

We evaluated the corresponding cell viability rate (%) in parallel experiments (i.e. using separated dishes) by adding 1.5 µM PI to the cells 2 h after the laser treatment. No PI was added before the laser treatment. In this case, the PI uptake indicates only cell death at a given laser fluence:

Viability rate (%) = (No. of red cells/No. of green cells) × 100%, time of PI addition: 2 h after laser treatment.

We counted the red cells at the centre of the laser irradiated area. The cell detachment was taken

into account by comparing to equivalent untreated cell areas. ImageJ software was used to process fluorescence microscopy images and perform cell counting. Three independent experiments for perforation and viability were performed in separate dishes. Perforation control experiments were carried out without adding AuNPs to the cells. Error bars represent the standard deviation of those experiments.

We used pump-probe shadowgraphic imaging implemented in upright microscope configuration for bubble detection. The setup was based on the electronic synchronization of the fs laser (pump) with a ns laser (probe) (Quantel) at 10 Hz. The ns probe pulses (λ = 532 nm, τ = 6 ns) were first directed to excite a fluorescent dye (rhodamine) solution. The technique allows for high quality imaging due to the emission of incoherent light from the dye (broad peak centered around 590 nm, $\tau \sim$ 6 ns). An IMI Teck IMB-17FT CCD camera and a long working distance 50X objective lens (Mitutoyo, numerical aperture (NA) of 0.55) were used for the imaging. Pictures of bubbles were taken using a 20 ns delay for the probe beam. The experimental methodology that enables bubble detection around single AuNP has been analytically described elsewhere [16]. For DF imaging, an external fiber illumination source was adapted sidelong to the cell samples. Switching between DF and pump-probe illumination was possible for an area of interest. Therefore, PB generation was directly linked to the presence of the AuNP on the cell membrane. For SEM characterization, cells were incubated with 8 µg/mL AuNPs during 3 h. Then, cells were washed three times with PBS, fixed in 5% glutaraldehyde/95% PBS for 0.5 h, then incubated in 5% glutaraldehyde/95% water for 0.5 h. The samples were then washed three times with distilled water and dried overnight under a biological hood. A 5 nm uniform gold layer was deposited on the samples using a sputter coater (Polaron Instruments). The samples were observed with a Hitachi S-4700 Field Emission SEM.

3. Results and discussion

SEM investigation confirmed the presence of single AuNPs and AuNP clusters on the cell surface (Figure 1(a, b)). We consider the washing of the dish with PBS as the dominant AuNP aggregation factor since the presence of salt balances the stabilizing negative charge of the AuNP. We calculated 15 ± 10 AuNP clusters per cell. The number of AuNPs per cell organized in clusters was 43 ± 30, which represented 57% of the total AuNPs per cell (76 ± 43). According to SEM, the AuNPs covered 0.52% of the cell surface and the total number of measured AuNPs represented 20.5% of the initially injected AuNPs. Living cells were imaged under both DF and pump-probe modes. Figure 1(c, d) show representative DF images of a cell sample at low and high magnification, respectively. The characteristic bright spots indicate the localization of the AuNPs on the cell membrane. AuNP clusters are generally linked to the brightest spots (white arrows in Figure 1(d)) due to their increased scattering cross-section compared to single AuNPs [17].

DF images prior to laser irradiation are compared with pump-probe shadowgraphic images of the same area, captured 20 ns after the laser irradiation with a single fs pulse at 200 mJ/cm^2 (Figure 1(e, f)). The measured PB diameter (D) varied from ~1 to 5 µm. The number of PB per cell is in agreement with the number of bubble nucleation spots observed by SEM (i.e., single AuNP and AuNP clusters). We have recently reported both theoretically and experimentally that laser irradiation of single 100 nm AuNP results in the generation of 0.9–1.4 µm bubbles for the examined laser fluence range [15]. Therefore, we attribute the observed relative large PB (> 1.4 µm) to the existence of "hot spots" within the assembly of AuNP clusters. Based on the observed PB size dispersion, DF spots can be linked with PB generated by either single AuNPs or AuNP clusters. Figure 1(d, f) reveal that both single AuNPs
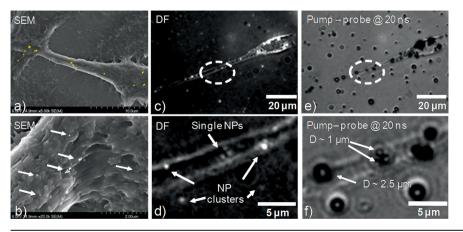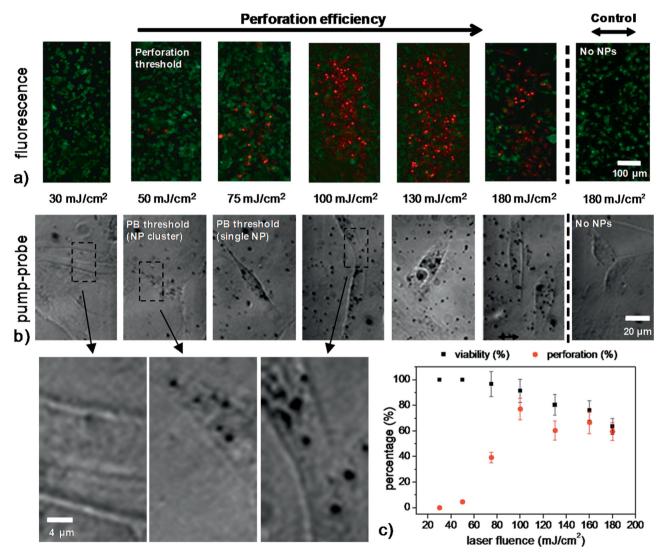

Figure 1 Cancer cells under (**a**)–(**b**) SEM imaging before laser irradiation, (**c**)–(**d**) DF microscopy before laser irradiation, (**e**)–(**f**) pump-probe shadowgraphic microscopy, 20 ns after the irradiation with a single 45 fs laser pulse at 200 mJ/cm^2.

and AuNP clusters generate PBs with almost 100% efficiency. The number of the bubbles linked to AuNP clusters was calculated to be 23 ± 7 per cell using the bubble size criterion. This is in agreement with the corresponding number of AuNP clusters (15 ± 10) quantified by SEM. In addition, pump-probe experiments demonstrated that 47% of the bubbles were generated by AuNP clusters, while 53% by single AuNPs. Since cell viability was low for single pulse irradiation at 200 mJ/cm^2, next experiments were conducted at lower laser fluences.

Figure 2(a) shows fluorescence microscopy images of cells treated with single fs laser pulse at fluences ranging from 30 to 180 mJ/cm^2. The uptake of the membrane impermeant PI indicates cell membrane perforation threshold of 50 mJ/cm^2. Single laser pulse irradiation at 100 mJ/cm^2 is the optimal treatment condition since the high perforation efficiency (77%) is accompanied with 90% cell viability. Control experiments (irradiation of cells without AuNPs) indicated no cell membrane perforation for the highest examined fluence of 180 mJ/cm^2 (Figure 2(a)).

The corresponding pump-probe images were captured for the examined laser fluence range (Figure 2(b)). The perforation threshold is in agreement with the observed bubble generation threshold at 50 mJ/cm^2. The latter strongly indicates that bubble

Figure 2 (**a**) Fluorescence microscopy images of cancer cells following treatment with a single 45 fs laser pulse at fluences ranging from 30 to 180 mJ/cm^2. Cell membrane was stained with WGA (green dye) and PI (red dye) was used as a perforation indicator. (**b**) Corresponding PB detection with pump-probe imaging at the examined laser fluences. The last column presents control perforation and PB detection experiments (without AuNPs) at 180 mJ/cm^2. Three insets show magnified pictures taken under laser fluences of interest. (**c**) Cell perforation and viability percentages dependency on the laser fluence.

generation and expansion is the key mediator for the perforation of the cell membrane. According to our recent work [16], single pulse laser irradiation at 50 mJ/cm^2 is not sufficient to generate a bubble around a single 100 nm AuNP. Therefore, considering the DF and SEM analysis, we hypothesize that only AuNP clusters contribute to the bubble generation and cell perforation at 50 mJ/cm^2. Higher laser fluence ($\geq 75 \text{ mJ/cm}^2$) results in the generation of submicron bubbles from single AuNPs, thus providing more disruption sites homogeneously distributed across the cell membrane. However, considerable cell death (38%) was observed for the laser fluence of 180 mJ/cm^2. Since 100 nm AuNPs present low absorption cross-section at 800 nm, we consider negligible contribution of thermal effects in the cell death. Cell death is mainly attributed to the observed bubbles of relative large size ($>5 \text{ μm}$) generated from the AuNP clusters. The expansion of those bubbles causes significant fluid flow that builds up a bubble wall shear stress on the order of tenths of kPa [18, 19], which has been reported to cause cell lysis [20]. Nor bubble generation or cell death has been observed for the control samples (without AuNPs) irradiated at 180 mJ/cm^2.

Since the development of laser based approaches for cell perforation and transfection aims to *in vivo* applications, we further discuss their efficiency in terms of the minimum required energy dose for cell treatment. The results between different studies are difficult to compare since cell perforation is affected by multiple parameters such as AuNP concentration, cell type, incubation time, laser type and perforation probe. Up to date, there are no studies dealing with single off-resonance excitation of AuNPs for cell perforation. Using multiple ultrafast pulses, Baumgart et al. [7] reported a pulse train of ~185 pulses at 60 mJ/cm^2 ($\tau = 45 \text{ fs}$, $\lambda = 800 \text{ nm}$) as the threshold value for cell perforation using 100 nm AuNPs. In a recent study, Schomaker et al. [12] reported a pulse train of 75 pulses at 50 mJ/cm^2 ($\tau = 120 \text{ fs}$, $\lambda = 800 \text{ nm}$) as the lowest value for membrane perforation using 200 nm AuNPs. Our living-cell bubble detection results demonstrate that those pulse trains are sufficient for bubble generation from small AuNP clusters. We can hypothesize that the first pulse possibly played the crucial role for the cell membrane perforation due to the excitation of the AuNP clusters. We recently observed that the first pulse of a pulse train induces a dynamic bubble expansion, which can break the AuNP clusters [16]. We may then assume that the subsequent pulses are less effective in terms of PB generation and can be eventually eliminated in a single pulse optimized process. Indeed, we observed cell membrane perforation using ~70 times less total laser energy comparing to the most effective off-resonance conditions [12]. The positively charged PI used in this work as perforation indicator may have also contributed in achieving such a low laser energy treatment. The PI molecules are expected to experience electrostatic attraction to the negatively charged cell membrane. In contrast, the negatively charged Lucifer Yellow used in previous studies [7, 12] is possibly subjected to charge repulsion to cell membrane. In the on-resonance approach, single laser pulse irradiation at 150 mJ/cm^2 ($\tau = 0.5 \text{ ns}$, $\lambda = 532 \text{ nm}$) has been reported sufficient for delivering cDNA in human stem cells, where PB generation has also been verified as the necessary condition for the cell membrane perforation [9]. In this study, the perforation was carried out using large molecules as probes, which require larger membrane pores to diffuse into the cytoplasm [12]. Our approach presents very promising potential to reduce significantly the required total energy dose for the cell membrane perforation using NIR fs laser pulses. This must be further investigated using other biomolecules such as small interfering RNA and plasmids. In future studies, the control of the AuNP aggregation can offer an additional optimization pathway. This might be achieved by varying the salt concentration, the AuNP surface functionalization and/or the AuNP incubation time with cells.

4. Conclusion

We demonstrated reversible perforation of the membrane of human breast cancer cells using plasmonic AuNP enhanced single NIR fs laser pulse. Ultrafast imaging demonstrated that the generation of submicron bubbles is the necessary condition for the perforation of the cell membrane. Interestingly, the minimum energy dose for cell perforation was reduced comparing to multiple pulses studies. The latter can be the basis for further development of AuNP enhanced cell perforation and transfection methods towards the implementation of an effective laser therapeutic tool for safe *in vivo* treatments.

References

[1] M. Giacca and S. Zacchigna, J. Control. Release **161**(2), 377–388 (2012).

[2] Y. Zhang and L.-C. Yu, BioEssays **30**(6), 606–610 (2008).

[3] M. Antkowiak, M. L. Torres-Mapa, D. J. Stevenson, K. Dholakia, and F. J. Gunn-Moore, Nat. Protoc. **8**(6), 1216–1233 (2013).

[4] J. Gehl, Acta Physiol. Scand. **177**(4), 437–447 (2003).

[5] C. M. Pitsillides, E. K. Joe, X. Wei, R. R. Anderson, and C. P. Lin, Biophys. J. **84**(6), 4023–4032 (2003).

[6] C. Yao, R. Rahmanzadeh, E. Endl, Z. Zhang, J. Gerdes, and G. Hüttmann, J. Biomed. Opt. **10**(6), 064012 (2005).

[7] J. Baumgart, L. Humbert, É. Boulais, R. Lachaine, J.-J. Lebrun, and M. Meunier, Biomaterials **33**(7), 2345–2350 (2012).

[8] D. Heinemann, M. Schomaker, S. Kalies, M. Schieck, R. Carlson, H. Murua Escobar, T. Ripken, H. Meyer, and A. Heisterkamp, PLoS ONE **8**(3), 58604 (2013).

[9] E. Y. Lukianova-Hleb, A. P. Samaniego, J. Wen, L. S. Metelitsa, C.-C. Chang, and D. O. Lapotko, J. Control. Release **152**(2), 286–293 (2011).

[10] B. St-Louis Lalonde, É. Boulais, J.-J. Lebrun, and M. Meunier, Biomed. Opt. Express **4**(4), 490–499 (2013).

[11] W. Ding, E. Bergeron, R. Lachaine, and M. Meunier, In: Applications of Nanoscience in Photomedicine, M. R. Hamblin and P. Avci, eds, Sawston (Cambridge, UK): Woodhead Publishing Limited, 331–376 (2015).

[12] M. Schomaker, D. Killian, S. Willenbrock, D. Heinemann, S. Kalies, A. Ngezahayo, I. Nolte, T. Ripken, C. Junghanß, H. Meyer, H. Murua Escobar, and A. Heisterkamp, J. Biophotonics, in press (2015).

[13] M. Schomaker, J. Baumgart, A. Ngezahayo, J. Bullerdiek, I. Nolte, H. Murua Escobar, H. Lubatschowski, and A. Heisterkamp, Proc. of SPIE **7192**, 71920U (2009).

[14] E. Boulais, R. Lachaine, A. Hatef, and M. Meunier, J. Photochem. Photobiol. C: Photochem. Rev. **17**, 26–49 (2013).

[15] E. Boulais, R. Lachaine, and M. Meunier, Nano Lett. **12**(9), 4763–4769 (2012).

[16] C. Boutopoulos, M. Fortin-Deschênes, E. Bergeron, and M. Meunier, Proc. of SPIE **8972**, 897208 (2014).

[17] M. Aioub, B. Kang, M. A. Mackey, and M. A. El-Sayed, J. Phys. Chem. Lett. **5**(15), 2555–2561 (2014).

[18] Y. Arita, M. Ploschner, M. Antkowiak, F. Gunn-Moore, and K. Dholakia, Opt. Lett. **38**(17), 3402–3405 (2013).

[19] K. R. Rau, P. A. Quinto-Su, A. N. Hellman, and V. Venugopalan, Biophys. J. **91**(1), 317–329 (2006).

[20] S. Peeters, M. Kitz, S. Preisser, A. Wetterwald, B. Rothen-Rutishauser, G. N. Thalmann, C. Brandenberger, A. Bailey, and M. Frenz, Biomed. Opt. Express **3**(3), 435–446 (2012).